A New Architecture for Direct Drive Robots

H. Kazerooni
S. Kim

Mechanical Engineering Department
University of Minnesota
Minneapolis, MN 55455

Abstract

A practical architecture, using a four-bar-linkage, is considered for the University of Minnesota direct drive robot [8]. This statically-balanced direct drive robot has been constructed for stability analysis of the robot in constrained manipulation. [3- 7]. As a result of the elimination of the gravity forces (without any counter weights), smaller actuators and consequently smaller amplifiers were chosen. The motors yield acceleration of 5g at the end point without overheating. High torque, low speed, brush-less AC synchronous motors are used to power the robot. Graphite epoxy composite material is used for the construction of the robot links. A 4-node parallel processor has been used to control the robot. The dynamic tracking accuracy -with the computed torque method as a control law- has been derived experimentally.

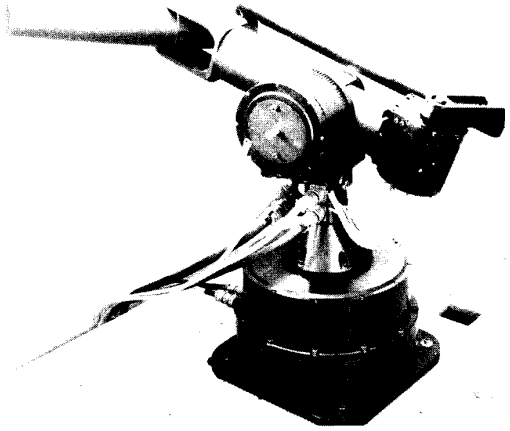

Figure 1: University of Minnesota Direct Drive Arm

Architecture

The architecture of this arm is such that the gravity term is completely eliminated from the dynamic equations. This balanced mechanism is designed without adding any extra counterbalance weights. The new features of this new design are as follows:

I. Since the motors are never affected by gravity, the static load will be zero. Hence no overheating results in the system in the static case.

II. Because of the elimination of the gravity terms, smaller motors with less stall torque (and consequently smaller amplifiers) have been chosen for a desired acceleration.

III. Because of the lack of gravity terms, higher accuracy can be achieved. This is true because the links have steady deflection due to constant gravity effect. This will give better accuracy and repeatability for fine manipulation tasks.

IV. As depicted in Figure 3, the architecture of this robot allows for a "large" workspace. The horizontal workspace of this robot is quite attractive from the stand point of manufacturing tasks such as assembly and deburring.

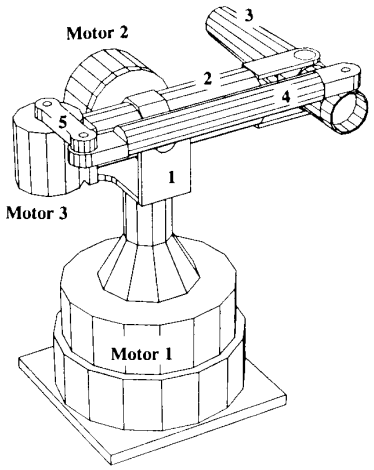

Figure 2: Schematic of University of Minnesota Arm

Figure 2 shows the schematic diagram of the University of Minnesota direct drive arm. The arm has three degrees of freedom, all of which are articulated drive joints. Motor 1 powers the system about a vertical axis. Motor 2 pitches the entire four-bar-linkage while motor 3 is used to power the four-bar-linkage. Link 2 is directly connected to the shaft of motor 2. Figure 3 shows the top view and side view of the robot. The coordinate frame $X_iY_iZ_i$ has been assigned to link i of the robot for i=1,2,..,5. The center of coordinate frame $X_1Y_1Z_1$ corresponding to link 1 is located at point 0 as shown in figure 3. The center of the inertial global coordinate frame $X_0Y_0Z_0$ is also located at point 0 (The global coordinate frame is not shown in the figures). The joint angles are represented by θ_1, θ_2, and θ_3. θ_1 represents the rotation of link 1; coordinate frame $X_1Y_1Z_1$ coincides on global coordinate frame $X_0Y_0Z_0$

when θ_1=0. θ_2 represents the pitch angle of the four-bar-linkage as shown in figure 3. θ_3 represents the angle between link 2 and link 3. Shown are the conditions under which the gravity terms are eliminated from the dynamic equations.

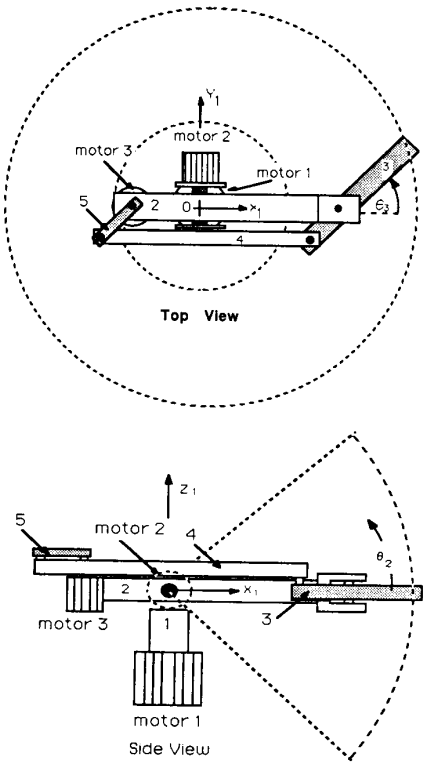

Figure 3: The Side View and Top View of the Robot

Figure 4 shows the four-bar-linkage with assigned coordinate frames. By inspection the conditions under which the vector of gravity passes through origin, 0, for all possible values of θ_1 and θ_3 are given by equations 1 and 2.

$$[\, m_3\bar{x}_3 - m_4L_5 - m_5\bar{x}_5 \,] \sin\theta_3 = 0 \qquad (1)$$

$$g\,(mt_3 + m_5) - m_2\bar{x}_2 - m_3(L_2 - g) - m_4(\bar{x}_4 - g\,) - [\, m_3\bar{x}_3 - m_4L_5 - m_5\bar{x}_5 \,]\cos\theta_3 = 0 \qquad (2)$$

where:
m_i, L_i = mass and length of each link,
$\bar{x}_i$ = the distance of center of mass from the origin of each coordinate frame,
mt_3 = mass of motor 3.
Conditions 1 and 2 result in:

$$m_3\bar{x}_3 - m_4L_5 - m_5\bar{x}_5 = 0 \qquad (3)$$

$$g(mt_3 + m_5) - m_2\bar{x}_2 - m_3(L_2 - g) - m_4(\bar{x}_4 - g\,) = 0 \qquad (4)$$

If equations 3 and 4 are satisfied, then the center of gravity of the four-bar-linkage passes through point 0 for all the possible configurations of the arm. Note that the gravity force still passes through 0 even if the plane of the four-bar-linkage is tilted by motor 2 for all values of θ_2.

Since at low speeds, AC torque motors do not tend to cog, low speed, high torque, and brush-less AC synchronous motors have been chosen to power the robot. Each motor consists of a ring shaped stator and a ring shaped permanent magnet rotor with a large number of poles. The rotor is made of rare earth magnetic material (Neodymium) bonded to a low carbon steel yoke with structural adhesive. The stator of the motor (with winding) is fixed to the housing for heat dissipation.

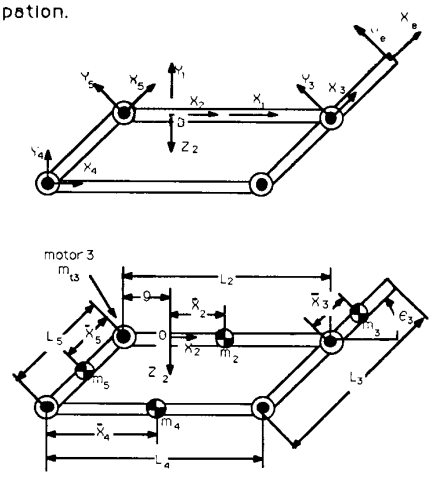

Figure 4: Four Bar link Mechanism

Forward Kinematics

The forward kinematic problem is to compute the position of the end point in the global coordinate frame $X_0Y_0Z_0$, given the joint angles, θ_1, θ_2, and θ_3. The end point position of the robot relative to the global coordinate frame is characterized by P_x, P_y, and P_z in the global coordinate frame $X_0Y_0Z_0$:

$$P_x = (C_1C_2C_3 - S_1S_3)(L_3 - L_5) + C_1C_2(L_2 - g) \qquad (5)$$

$$P_y = (S_1C_2C_3 + C_1S_3)(L_3 - L_5) + S_1C_2(L_2 - g) \qquad (6)$$

$$P_z = S_2(L_2 - g) + S_2C_3(L_3 - L_5) \qquad (7)$$

where $S_i = \sin(\theta_i)$, and $C_i = \cos(\theta_i)$.

Inverse Kinematics

The inverse kinematic problem is to calculate the joint angles for a given end point positionwith respect to the global coordinate frame. The closed-form of inverse kinematics of the proposed arm derived using the standard method[2,11]. The joint angles for the given end point position can be determined using the following equations:

$$\theta_1 = \text{atan2}(P_y, P_x) - \text{atan2}\left((L_3 - L_5)\sin\theta_3,\ \pm\sqrt{P_x^2 + P_y^2 - (L_3 - L_5)^2\sin^2\theta_3}\,\right) \qquad (8)$$

$$\theta_2 = \sin^{-1}\left(\frac{P_z}{(L_2 - g) + (L_3 - L_5)\cos\theta_3}\right) \qquad (9)$$

$$\theta_3 = \cos^{-1}\left(\frac{P_x^2 + P_y^2 + P_z^2 - (L_2 - g)^2 - (L_3 - L_5)^2}{2(L_2 - g)(L_3 - L_5)}\right) \qquad (10)$$

Dynamics

The closed-form dynamic equations have been derived for the purpose of controller design. The dynamic behavior of the arm can be presented by the following equation [1,2]

$$M(\theta)\ddot{\theta} + CE(\theta)[\dot{\theta}^2] + CO(\theta)[\dot{\theta}\dot{\theta}] + G(\theta) = \tau \qquad (11)$$

Where:

$\tau = [\tau_1\ \tau_2\ \tau_3]^T$ 3×1 vector of the motor torques,

$M(\theta)$ 3×3 definite inertia matrix,

$CE(\theta)$ 3×3 centrifugal coefficients matrix,

$CO(\theta)$ 3×3 Coriolis coefficients matrix,

$G(\theta)$ 3×1 vector of gravity force,

$\ddot{\theta}$ $[\ddot{\theta}_1\ \ddot{\theta}_2\ \ddot{\theta}_3]^T$

$[\dot{\theta}\dot{\theta}]$ $[\dot{\theta}_1\dot{\theta}_2\quad \dot{\theta}_1\dot{\theta}_3\quad \dot{\theta}_2\dot{\theta}_3]^T$

$[\dot{\theta}^2]$ $[\dot{\theta}_1^2\quad \dot{\theta}_2^2\quad \dot{\theta}_3^2]^T$

$$M(\theta) = \begin{bmatrix} M_{11} & M_{12} & M_{13} \\ M_{12} & M_{22} & 0 \\ M_{13} & 0 & M_{33} \end{bmatrix},\quad CE(\theta) = \begin{bmatrix} 0 & CE_{12} & CE_{13} \\ CE_{21} & 0 & 0 \\ CE_{31} & CE_{32} & 0 \end{bmatrix}$$

$$CO(\theta) = \begin{bmatrix} CO_{11} & CO_{12} & CO_{13} \\ 0 & CO_{22} & CO_{23} \\ CO_{31} & 0 & 0 \end{bmatrix},\quad G(\theta) = \begin{bmatrix} 0 \\ 0 \\ 0 \end{bmatrix}$$

$$M_{11} = I_{z1} + C_2^2(I_{e1} + I_{e6} + I_{e2} + 2C_3 I_{e3} + I_{y2} + m_2\bar{x}_2^2) + S_2^2(S_3^2(I_{e1} + I_{e5}) + C_3^2 I_{e4} + I_{x2})$$

$$M_{12} = S_2S_3(I_{e3} + C_3(I_{e1} + I_{e5} - I_{e4}))$$

$$M_{13} = C_2(I_{e1} + I_{e6} + C_3 I_{e3})$$

$$M_{22} = I_{z2} + m_2\bar{x}_2^2 + C_3^2(I_{e1} + I_{e5}) + S_3^2 I_{e4} + I_{e2} + 2C_3 I_{e3}$$

$$M_{33} = I_{e1} + I_{e6}$$

$$CE_{12} = C_2S_3(I_{e3} + C_3(I_{e1} + I_{e5} - I_{e4}))$$

$$CE_{13} = -C_2S_3 I_{e3}$$

$$CE_{21} = S_2C_2(I_{y2} - I_{x2} + m_2\bar{x}_2^2 - S_3^2 I_{e5} + C_3^2(I_{e1} - I_{e4}) + I_{e2} + I_{e6} + 2C_3 I_{e3})$$

$$CE_{31} = S_3(C_2^2 I_{e3} - S_2^2 C_3(I_{e1} + I_{e5} - I_{e4}))$$

$$CE_{32} = S_3(I_{e3} + C_3(I_{e1} + I_{e5} - I_{e4}))$$

$$CO_{11} = -2CE_{21}$$

$$CO_{12} = -2CE_{31}$$

$$CO_{13} = -S_2(2S_3^2 I_{e1} + I_{e6} + \cos 2\theta_3(I_{e4} - I_{e5}))$$

$$CO_{22} = S_2(2C_3^2 I_{e1} + I_{e6} + 2C_3 I_{e3} - \cos 2\theta_3(I_{e4} - I_{e5}))$$

$$CO_{23} = -2CE_{32}$$

$$CO_{31} = -S_2(I_{e1} + \cos 2\theta_3(I_{e1} + I_{e5} - I_{e4}) + I_{e6} + 2C_3 I_{e3})$$

where:

$$I_{e1} = m_3\bar{x}_3^2 + m_4 L_5^2 + m_5\bar{x}_5^2$$

$$I_{e2} = m_3(L_2 - g)^2 + m_4(\bar{x}_4 - g)^2 + m_5 g^2$$

$$I_{e3} = m_3\bar{x}_3(L_2 - g) - m_4(\bar{x}_4 - g)L_5 + m_5\bar{x}_5 g$$

$$I_{e4} = I_{x3} + I_{x4} + I_{x5}$$

$$I_{e5} = I_{y3} + I_{y4} + I_{y5}$$

$$I_{e6} = I_{z3} + I_{z4} + I_{z5}$$

I_{xi}, I_{yi}, and I_{zi} are the mass moments of inertia relative to x, y, z axis at the center of mass of a link i. (motor 3 is a part of link 2). The gravity term, $G(\theta)$ becomes zero when equations 3, 4 are satisfied in the arm. This condition holds for all possible configurations.

Hardware

An IBM AT microcomputer which is hosting a 4-node parallel processor is used as the main controller of this robot. The parallel processor has four nodes and a PC/AT bus interface. Each node is an independent 32-bit processor with local memory and communication links to the other nodes in the system. A high speed AD/DA converter has been used for reading the velocity signals and sending analog command signals to the servo controller unit. A parallel IO board (D/D converter) between the servo controller unit and the computer allows for reading the R/D (Resolver to Digital) converter.

The servo controller unit produces three phase, Pulse Width Modulated (PWM), sinusoidal currents for the power amplifier. The servo controller unit contains an interpolator, R/D converter and a communication interface for the computer. The servo controller unit can be operated in either a closed loop velocity or current (torque) control mode (the current control is used). A PWM power amplifier, which provides up to 47 Amperes of drive current from a 325 volt power supply, is used to power the mortors. The main DC bus power is derived by full-wave rectifying the three phase 230VAC incoming power. This yields a DC bus voltage of 325VDC.

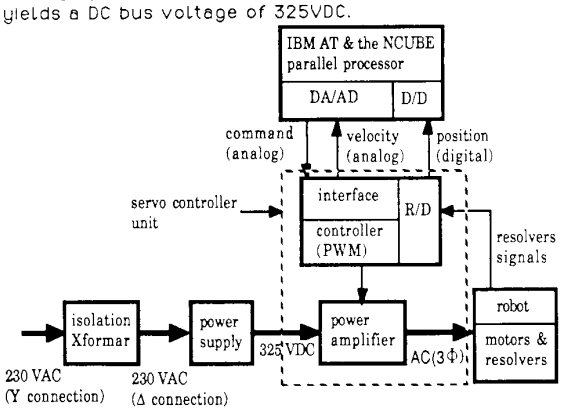

Figure 5: The Control Hardware for Minnesota Robot

The motors used in this robot are neodymium (NdFeB) magnet AC brushless synchronous motor. Due to the high magnetic field strength (maximum energy products: 35 MGOe) of the rare earth NdFeB magnets, the motors have high torque to weight ratio. Pancake type resolvers are used as position and velocity sensors. The peak torque of motor 1 is 118 Nm, while the peak torques of motors 2 and 3 are 78 and 58 Nm repectively.

The preliminary evaluation of the performance of robot concerns with the dynamic tracking accuracy along a specified trajectory. The computed torque method (9,10) is used to control the robot. While a nonlinear compensator for compensation of the feedforward terms is considered in the feedforward loop, a linear compensator in the feedback loop has been used to decrease the error in each joint. The inertia parameters used in feedforward loop are computed from the engineering drawings. The motor dynamics and the friction in the dynamic model were

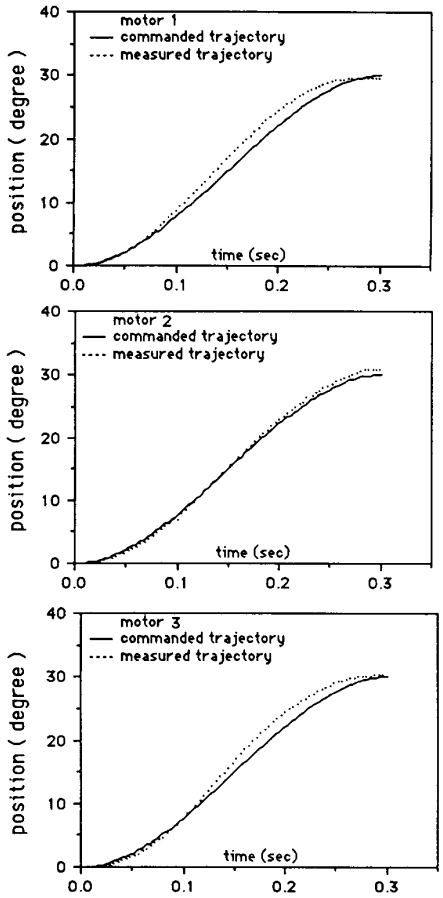

Figure 6: Position tracking curves with full robot motion

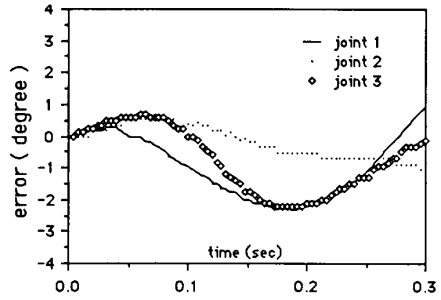

Figure 7: The error in each motor

neglected. The dynamic model does not include the gravity terms.

All the joints were commmanded simultaneously to start from origin to reach the position of 30 degree in 0.3 sec. The commanded trajectory is a cubic polynomial. The maximum velocity and acceleration for each joint are 150 degree/sec and 2000 degree/sec^2, respectively. The trajectory for each joint are depicted in figure 6. Figure 7 shows the error for each motor. The parameter identification algorithm to obtain a better estimate of the dynamic parameters is under study with the integrated dynamic model of the robot and motor. This will enable us to analyze the effect of parametric errors and the robustness of the computed torque technicque.

Summary

This paper presents some results of the on-going research project on statically-balanced direct drive arm at the University of Minnesota. The following features characterize this robot:

1. The statically-balanced mechanism without counter weights allows for selection of smaller actuators. Since in static or quasi-static operations, no load is on the actuators, therefore the overheating of the previous direct drive robots will be alleviated.
2. The robot links are made of graphite-epoxy composite materials to give more structural stiffness and less mass. The high structural stiffness and low mass of the links allow for the wide bandwidth of the control system.
3. Impedance control has been considered for control of the robot. The object of the control task is to develop a control system such that, this robot will be capable of maneuvering in constrained and unconstrained environments.

References

1. Asada, H. and Slotine, J.-J.E., "Robot Analysis and Control", John Wiley and Sons, 1986.
2. Craig, J. J., "Introduction to Robotics: Mechanics and Control, Addison-Wesley, Reading, Mass 1986.
3. Hogan, N., " Impedance Control, An Apptroach Manipulation", ASME Journal of Dynamic Systems, Measurement, and Control, March, 1985.
4. Kazerooni, H., Sheridan, T., B., Houpt, P. K., "Fundamentals of Robust Compliant Motion for Robot Manipulators" , IEEE Journal on Robotics and Automation, vol. 2, NO. 2, June 1986.
5. Kazerooni, H., Houpt, P. K., Sheridan, T., B., " Design Method for Robust Compliant Motion for Robot Manipulators", IEEE Journal on Robotics and Automation, vol. 2, NO. 2, June 1986.
6. Kazerooni, H., "Robust Non-linear Impedance Control", In proceedings of the IEEE International Conference on Robotics and Automation, Raleigh, North Carolina, April 1987.
7. Kazerooni, H., Beikovicius, J., Guo, J., "Compliant Motion Control for Robot Manipulators, Input Output Approach", In proceeding of the American Control Conference, June 1987, Minneapolis.
8. Kazerooni, H., Kim, S., "Statically Balanced Direct Drive Robot for Compliance Control Analysis", presented at ASME Winter Annual Meeting, "Modeling and Control of Robotic Manipulators and Manufacturing Processes", Boston, 1987.
9. Luh, J. Y. S., Walker, M. W. and Paul, R. P., "Resolved - Acceleration Control of Mechanical Manipulators", IEEE Transactions on Automatic Control 25 (3) June, 1980, pp 468 - 474.
10. Markiewicz, B. R., "Analysis of the Computed Torque Drive Method and Comparision with the Conventional Position Servo for a Computer - Controlled Manipulator", Technical Memorandum 33 - 601, Jet pPropulsion Lab, Pasadena, CA, March, 1973.
11. Paul, R. P., Robot Manipulators: Mathematics, Programming, and Control", MIT press, Cambridge, Mass, 1981.